IOP PUBLISHING PHYSICS IN MEDICINE AND BIOLOGY

Phys. Med. Biol. **55** (2010) 2269–2280 doi:10.1088/0031-9155/55/8/010

Measurement of scattered radiation in a volumetric 64-slice CT scanner using three experimental techniques

A Akbarzadeh[1,2], M R Ay[1,2,3,7], H Ghadiri[2,4], S Sarkar[1,2] and H Zaidi[5,6]

[1] Department of Medical Physics and Biomedical Engineering, Tehran University of Medical Sciences, Tehran, Iran
[2] Research Center for Science and Technology in Medicine, Tehran University of Medical Sciences, Tehran, Iran
[3] Research Institute for Nuclear Medicine, Tehran University of Medical Sciences, Tehran, Iran
[4] Department of Medical Physics, Iran University of Medical Sciences, Tehran, Iran
[5] Division of Nuclear Medicine, Geneva University Hospital, CH-1211 Geneva, Switzerland
[6] Geneva Neuroscience Center, Geneva University, CH-1205 Geneva, Switzerland

E-mail: mohammadreza_ay@tums.ac.ir

Received 5 November 2009, in final form 3 February 2010
Published 30 March 2010
Online at stacks.iop.org/PMB/55/2269

Abstract

Compton scatter poses a significant threat to volumetric x-ray computed tomography, bringing cupping and streak artefacts thus impacting qualitative and quantitative imaging procedures. To perform appropriate scatter compensation, it is necessary to estimate the magnitude and spatial distribution of x-ray scatter. The aim of this study is to compare three experimental methods for measurement of the scattered radiation profile in a 64-slice CT scanner. The explored techniques involve the use of collimator shadow, a single blocker (a lead bar that suppresses the primary radiation) and an array blocker. The latter was recently proposed and validated by our group. The collimator shadow technique was used as reference for comparison since it established itself as the most accurate experimental procedure available today. The mean relative error of measurements in all tube voltages was 3.9 ± 5.5% (with a maximum value of 20%) for the single blocker method whereas it was 1.4 ± 1.1% (with a maximum value of 5%) for the proposed blocker array method. The calculated scatter-to-primary ratio (SPR) using the blocker array method for the tube voltages of 140 kVp and 80 kVp was 0.148 and 1.034, respectively. For a larger polypropylene phantom, the maximum SPR achieved was 0.803 and 6.458 at 140 kVp and 80 kVp, respectively. Although the three compared methods present a reasonable accuracy for calculation of the scattered profile in the region corresponding to the object, the collimator shadow method is by far the most accurate empirical technique. Nevertheless, the blocker array method

[7] Author to whom any correspondence should be addressed.

is relatively straightforward for scatter estimation providing minor additional radiation exposure to the patient.

(Some figures in this article are in colour only in the electronic version)

1. Introduction

The quantitative measurement of the local linear attenuation coefficient, or its correlates, has been a long-term objective since the introduction of early generation computed tomography (CT) scanners (Kalender 1988). However, despite the success of quantitative CT, the nonlinearity of projection data resulting from beam hardening, partial volume averaging and scattered radiation still spoil the reconstructed image quality and make robust quantitative measurements difficult to achieve in practice.

It has long been recognized that x-ray scatter poses a significant threat to CT scanning by further reducing soft tissue contrast (Tofts and Gore 1980). In addition, the contamination of CT data with scattered radiation reduces reconstructed CT numbers and introduces cupping artefacts in the reconstructed images (Kanamori *et al* 1985). This effect is more pronounced in the extended fan-beam geometry (multiple-row detector systems) and the cone-beam geometry (flat-panel detectors), which are much less immune to scatter than conventional fan-beam CT scanners (Siewerdsen and Jaffray 2001, Johns and Yaffe 1982, Glover 1982, Ohnesorge *et al* 1999, Colijn and Beekman 2004). It should be emphasized that scattered radiation reduces the attenuation coefficients and as such the calculated CT numbers are lower than the actual values for most biological tissues except lung tissues where scatter increases CT numbers. As the scatter component (magnitude and spatial distribution) is object dependent, the amount of scatter inherently present during the calibration procedure might not reflect the scatter typically encountered in various clinical exams. This problem has been addressed by several groups which have shown that cupping artefacts appear on reconstructed images of large homogeneous objects whereas streak artefacts appear in the form of dark bands or streaks in directions of high attenuation (Maltz *et al* 2008a, Ning *et al* 2004, Ohnesorge *et al* 1999). With the advent of extended fan- and cone-beam CT scanners equipped with either multi-row detector arrays or flat-panel detectors during the last decade, the problem of x-ray scatter was given more attention owing to the use of a large beam angle (Sorenson and Floch 1985, Siewerdsen and Jaffray 2000). Characterization of the magnitude and spatial distribution of scattered radiation in current and future generation CT scanners with the large beam angle is mandatory for optimization of scanner design and development of robust scatter correction techniques (Siewerdsen *et al* 2006). However, despite much worthwhile research and progress made during the past few years, this topic remains a challenging research area.

Scatter correction strategies in x-ray CT rely on one of the following approaches: knowledgeable selection of the object-to-detector gap (Ning *et al* 2004, Maltz *et al* 2008b), use of the collimator (septa) in the detector housing between detector elements directed towards the focal spot (Ohnesorge *et al* 1999, Bertram *et al* 2005, Zhu *et al* 2006, 2009, Rinkel *et al* 2007), assessment of scatter contribution behind dedicated beam stoppers (Johns and Yaffe 1982, Endo *et al* 2006, Ning *et al* 2004, Maltz *et al* 2008b) and algorithmic model-based correction procedures (Siewerdsen *et al* 2006, Glover 1982).

The latter approach requires an accurate estimation of the scatter-to-primary ratio (SPR) profile and hence the scatter component in the measured projection data (Johns and Yaffe 1982, Yao and Leszczynski 2009). A wide variety of techniques were developed to measure

or calculate the scatter component from raw CT data which can be divided into two major groups, namely empirical and model-based techniques. Empirical techniques include 'blocker-based' (Kanamori *et al* 1985, Endo *et al* 2001, Malusek *et al* 2003, 2008, Ay and Zaidi 2005, Zaidi and Ay 2007) and 'collimator-based' techniques (Ohnesorge *et al* 1999, Li *et al* 2008) whereas model-based techniques include analytical modelling (Endo *et al* 2006) and Monte Carlo simulation techniques (Yao and Leszczynski 2009, Zhu *et al* 2009). In addition to the aforementioned techniques, some researchers have proposed a hybrid 'convolution-based' approach which combines empirical and model-based techniques (Zaidi and Ay 2007).

Each of the above-mentioned techniques has pros and cons. Blocker-based techniques extract the scatter fluence directly from the projection data by blocking the primary photons and recording scattered radiation in the blocker shadow (Ay and Zaidi 2005, Malusek *et al* 2008). Since these techniques use a blocker with high attenuation coefficient and suitable size to stop the primary radiation covering a specific area of the phantom and detector, the blocker can be a source of scattered radiation. The secondary radiation induces some systematic error in the calculation. Moreover, based on theoretical calculations the blocker is not an ideal attenuator and cannot block the primary photons completely. Collimator-based techniques record scattered radiation in the collimator shadow and as such are assumed to be more accurate than blocker-based techniques. However, they are not suitable for use in the cone beam geometry. Model-based techniques estimate the contribution of scattered radiation using analytical or Monte Carlo modelling techniques. Analytical calculation of the scattered radiation distribution is fast but limited to simple models of patient shape and heterogeneity (Siewerdsen *et al* 2006). Monte Carlo modelling is by far the most accurate and robust approach to calculate scattered radiation distribution (Johns and Yaffe 1982); however, despite substantial progress in computing power, the technique remains computationally expensive and time consuming (Akbarzadeh *et al* 2008).

In this study, we measured the spatial distribution of scattered radiation and SPR in a GE LightSpeed VCT (General Electric Healthcare Technologies, Waukesha, WI, USA) 64-slice scanner with a detector coverage of 40 mm using three different experimental methods, including collimator-based (Johns and Yaffe 1982) and blocker-based techniques using a single (Akbarzadeh *et al* 2008) or an array (Ay and Zaidi 2005) of blockers. The latter approach was recently proposed by our group. To the best of our knowledge, a comparative analysis of various techniques for experimental measurement of x-ray scatter for latest generation cone-beam 64-slice CT scanners has not been reported before.

2. Materials and methods

2.1. CT scanner

The 64-slice GE LightSpeed VCT scanner (GE Healthcare Technologies, Waukesha, WI) with volumetric data acquisition capability was used. This third generation CT scanner has a z-axis resolution of up to 0.35 ± 0.05 mm and 44 ms temporal resolution for cardiac studies. The gantry aperture diameter is 700 mm, the distance between the focal spot and the isocentre (centre of the gantry) is 540 mm whereas the distance between the focal spot and the detector array is 950 mm. The gantry maximum scan field of view is 500 mm. This scanner is equipped with a Performix Pro100 anode grounded metal-ceramic x-ray tube. The tube has a dual focal spot with two (small and large) focal spots. The small focal spot's dimension is equal to 0.9 mm width $\times$ 0.7 mm length and can deliver at utmost 335 mA in a 0.4 s rotation. The large focal spot's dimension is equal to 1.2 mm width $\times$ 1.2 mm length and can deliver up to 900 mA in a 0.4 s rotation. The anode of this tube is made of tungsten and the target angle is 7°. The

tube has two kinds of filtration: first, the inherent filtration of tube referred to as the minimum Al equivalent at 70 kV for the tube housing and is 3.25 mm Al equivalent. Second, the added filtration consists of 0.1 mm of copper aiming at the reducing beam hardening effect and minimizing patient dose. The scanner's generator has a maximum output power of 100 kW. The generator is capable of producing four different tube voltages from 80 to 140 kVp. It can generate different tube currents ranging between 10 mA and 800 mA, with 5 mA increments.

The scanner takes advantage of the Highlight ceramic scintillator CT detector. As can be seen on the detector chemical formula ($Y_2Gd_2O_3$:Eu), it is composed of Gadolinium and Yttrium with impurity of Europium. The primary speed of this ceramic is about 10^{-3} s whereas the thickness needed to stop (x-ray stopping power) 98% of incident x-rays emanating from a typical 140 kVp CT beam is 3 mm. The crystal's light output (relative light signal at the diode for a given x-ray input) is 70% at 610 nm.

The detector array with the aperture size of 40 mm at the isocentre consists of 58 368 individual elements configured in 64 rows of 0.625 mm thickness in the z-direction and 0.55 mm in the x-direction at the isocentre, each containing 888 active patient elements and 24 reference elements. The data are acquired as 64 $\times$ 0.625 mm collimation, with the option of producing thicker slices during image reconstruction or through post-reconstruction image processing. The data acquisition system (DAS) includes 58 368 input channels with a 2460 Hz maximum sampling rate.

2.2. Phantoms

Two right cylindrical phantoms were used in the experimental setup: a small water-filled cylindrical phantom made of Perspex having an external diameter of 215 mm with a 6 mm wall thickness and a large solid polypropylene phantom having a diameter of 350 mm. The latter solid phantom is usually employed for modelling bony structures and is suitable for large field of views scanning.

2.3. Experimental measurement of scatter profiles

2.3.1. Collimator shadow method. Since the phantom is homogeneous in geometry and in content through the z-axis (cylindrical water-filled phantom), the scatter profile shows approximately a uniform pattern through the vertical direction of the fan plane (z-axis). Thus, in collimator shadow one may record the scatter pattern directly without the need for any particular correction. In order to do so, the beam aperture was restricted in such a way that only the central rows of the detector array were exposed. The outermost detector rows which lie on the collimator shadow on both sides record only scattered radiation (figure 1(a)). Hence the detector reading of such rows was extracted yielding the spatial distribution of scattered radiation (the details of detector reading extraction are given in section 2.3.4). In comparison with other techniques, the collimator shadow method can be considered as the most straightforward and immune to error.

2.3.2. Conventional single blocker method based on a lead bar as a primary blocker. This method was first proposed in the 1980s (Rinkel *et al* 2007, Akbarzadeh *et al* 2008). In this method, a lead cubic bar with dimensions of 2 $\times$ 2 $\times$ 10 cm is inserted exactly above the phantom to block the primary photons in a small shadowed area on the detector array (figure 1(b)). In order to get the complete scatter profile, the x-ray source and detector array were rotated around the phantom while the blocker and phantom are continuously exposed to the x-ray beam. The sinogram resulting from this exposure was extracted to an external PC

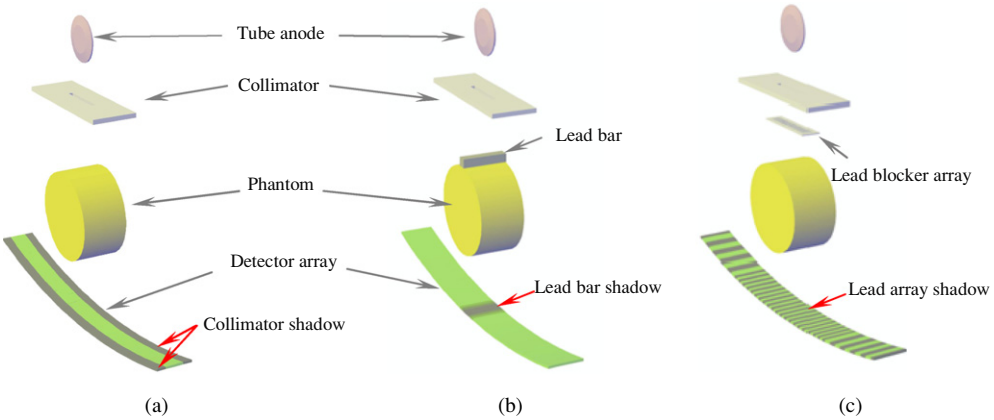

Figure 1. Schematic representation of the geometric configuration of experimental techniques assessed in this study. (a) Collimator shadow set-up; (b) conventional single blocker method; (c) lead blocker array setup.

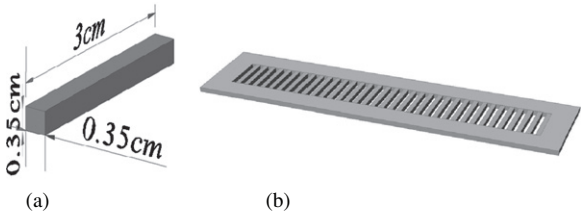

Figure 2. Schematic view of blockers used in the blocker-based method of scatter measurement: (a) dimensions of a single element of the blocker array; (b) the blocker array.

for analysis. Each profile of the sinogram consists of a small region of the shadowed area which carries scatter records of detectors and a large region of the irradiated area. A computer program was written in MatLab 7.6 (The MathWorks Inc., Natick, MA, USA) to extract the shadowed part of each view and dispose of the large region of the irradiated area separately for each profile. Therefore, we achieved a number of profiles, each containing scatter data in individual detector elements. The obtained profiles were merged to create the entire scatter profile by calculating the union of shadowed areas in all profiles. The correction for primary photons which passed the blocker was done using the blocker attenuation factor profile. This factor was obtained from exposure of the same configuration without the phantom in the field of view.

2.3.3. Lead blocker array method. The configuration in this study consists of several small lead bars in the form of an array. Each lead bar has dimensions of 30 mm length $\times$ 0.35 mm width $\times$ 0.35 mm height. The total number of lead bars is 26 and the blank space between these bars is equal to 0.35 mm. The above-mentioned dimensions of lead bars were chosen in such a way that they are large enough to block the primary photons and small enough to sample the scatter pattern accurately. The array plays the role of blocker for primary photons and is thus referred to as the blocker array. Figures 2(a) and (b) show the schematic views of a single lead bar used in an array and the complete blocker array.

The x-ray blocker array was placed beneath the x-ray second collimator to be imaged, as shown in figure 1(c). It should be noted that this novel technique was already validated in our previous study (Johns and Yaffe 1982). By adequately choosing the dimensions of the lead bars, each shadowed area in a projection image was as small as possible while completely blocking the primary x-ray photons. The intensity recorded on the detector array might be divided into two individual regions, shadowed area and irradiated area. The intensity detected within each shadowed area was assumed to be exclusively that of the scattered x-ray photons, resulting in the x-ray scatter distribution sampled on a sparse lattice. The scatter distribution was estimated by employing a spatial cubic sp-line interpolation on these samples. In order to extract primary photons distribution, the irradiated areas were first interpolated to yield the 'primary + scattered' distribution. Second, the scatter distribution was subtracted from the resulting distribution. This method was used to extract the SPR and scatter profiles.

2.3.4. Detector raw data extraction. Extraction of detector raw data, which are usually stored in encrypted manufacturer proprietary format, is a crucial step for implementation of the aforementioned experimental methods. This required reading out scanner raw data before application of system-specific correction procedures. Following x-ray exposure, the signal produced by any detector element enters a specific channel in the DAS and is converted to a digital signal by means of analog to digital converters (ADCs). Thereafter, the digital signals are written into a binary file. Since each exposure lasts few seconds, the DAS transfers the data frequently with a sampling rate of 2460 Hz. Hence, the DAS records the data from all detector arrays several times and each set is called a view. The recorded binary file containing all views is stored in 16 bit format.

A computer program and associated graphical user interface (GUI) were developed in MatLab 7.6 (The MathWorks Inc., Natick, MA, USA), whose kernel was capable of reading the binary data from the raw file and extracting a two-dimensional matrix (912 $\times$ 64) as output. To this end, the above-mentioned calibration factors were applied inversely to the output matrix to recover the real detectors read-out. These calibration factors were calculated through several experimental studies using a dedicated phantom. Moreover, the GUI enables the user to extract raw data and save the output matrix as Excel worksheet, MatLab data file or binary format.

2.4. Comparison strategy

The scatter profiles measured by both the single and array blockers were compared with results derived from the collimator shadow technique used as reference. The normalized error (NE) was used as a figure of merit to evaluate differences between two data sets (Zaidi and Ay 2007):

$$NE(u, v) = \frac{P_{\text{measured}}(u, v) - P_{\text{reference}}(u, v)}{P_{\text{reference}}(u, v)}, \tag{1}$$

where u and v are detector element coordinates, and $P_{\text{measured}}(u,v)$ and $P_{\text{reference}}(u,v)$ are the measured and reference (collimator shadow) projection data for each detector element, respectively.

3. Results

Figure 3 shows the scatter profiles measured using the three experimental techniques including the collimator shadow, single blocker and lead blocker array for detector row no 32 (central

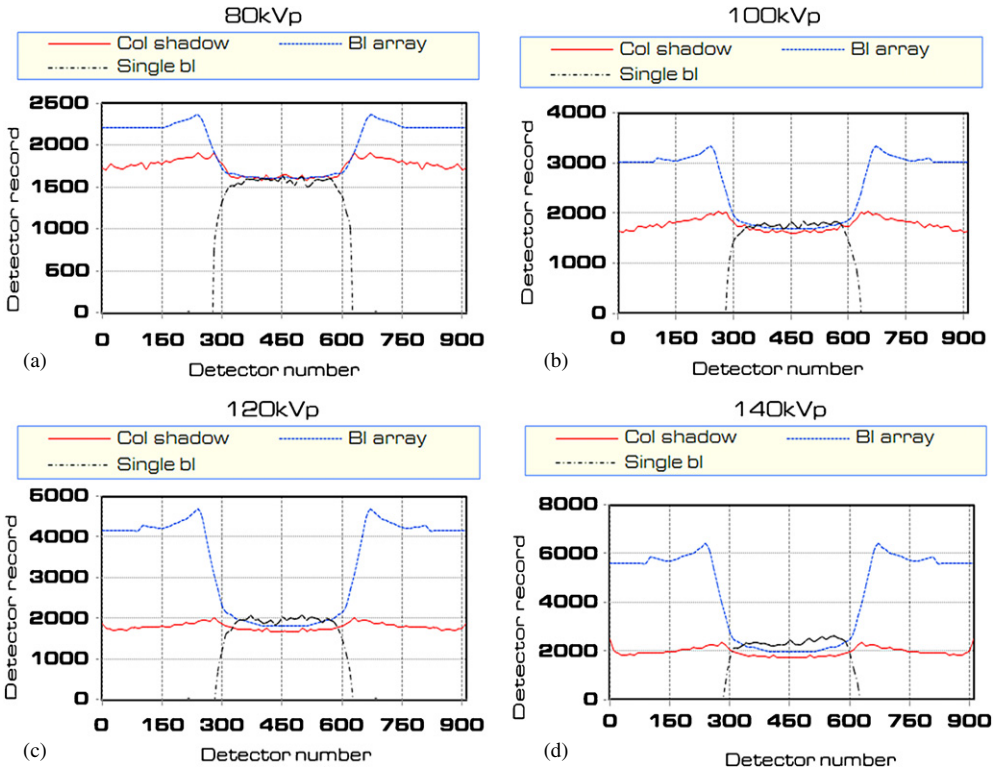

Figure 3. Recorded energy fluence of scattered radiation for a single detector row estimated using the three experimental techniques under conditions of the 100 mA tube current for a cylindrical water-filled phantom: (a) 80 kVp; (b) 100 kVp; (c) 120 kVp; (d) 140 kVp.

row) at different tube voltages. In these measurements, the water-filled phantom was exposed to 100 mA tube current. It should be noted that the bowtie filter was removed during the measurements. Hence, the scatter profiles reflect the real output of the detectors (the deposited energy in detector elements) without normalization. The scatter profiles are quite similar in the region corresponding to the phantom shadow; however, noticeable discrepancy can be observed outside this region owing to differences in the experimental setup used by the various methods. Blocker-based techniques record a high contribution of primary contamination (primary photons crossing the blocker) outside the phantom shadow. In contrast, the collimator shadow technique is more accurate owing to its high efficiency for stopping primary photons using the collimator aperture. This is the motivation behind its use as reference for comparison in this study. Figure 4 shows the normalized errors for different kVps obtained by comparing the collimator shadow method with the two other experimental techniques limited to the region of the collimator shadow. All comparisons were merely performed in the phantom shadow region (detector elements 300–600).

Figure 5(a) presents the SPR profile for the cylindrical water-filled phantom (ϕ = 210 mm) at different tube voltages (between 80 kVp and 140 kVp) and 100 mA tube current. Likewise, figure 5(b) shows the SPR profiles for the polypropylene phantom (ϕ = 350 mm) calculated at various tube voltages and 200 mA tube current in order to decrease statistical fluctuations of measured data owing to the absorption of photons in the polypropylene phantom (figure 5(b)). The bowtie filter was removed for both measurements. It should be emphasized

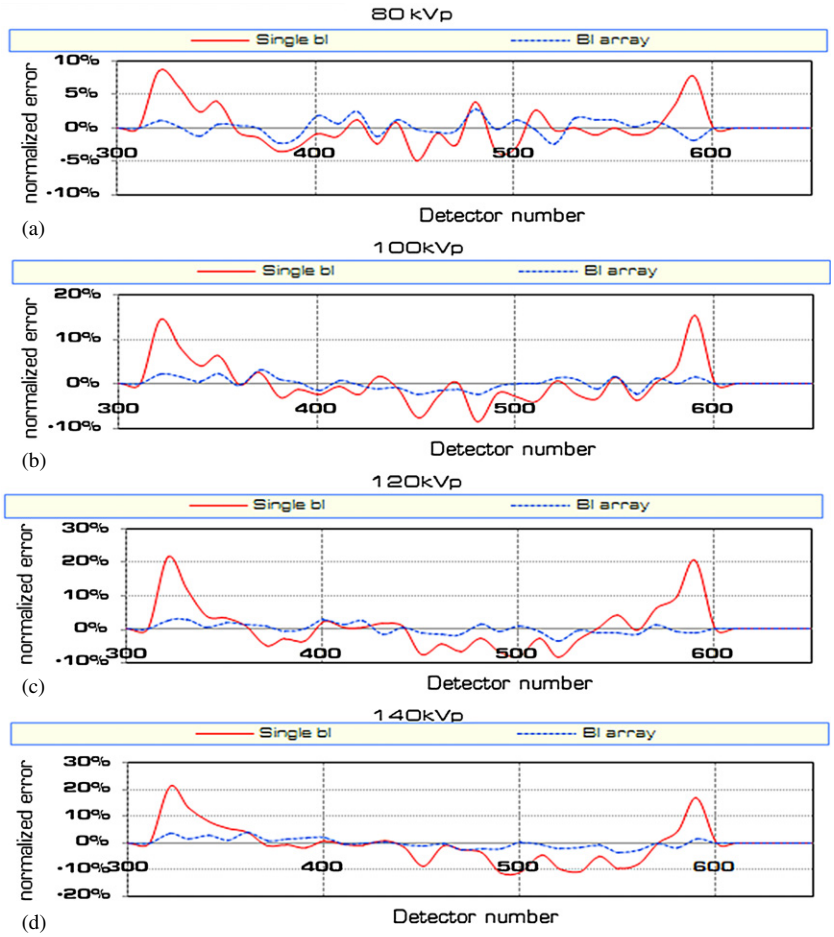

Figure 4. Comparison between the collimator shadow method and the other two experimental techniques for the scatter component estimated in the shadow area of the phantom (detector elements from 300 up to 600). The normalized relative error is reported for (a) 80 kVp; (b) 100 kVp; (c) 120 kVp (d) 140 kVp.

that the profiles in figure 5 belong to detector row no 32. The maximum measured SPR for both water and polypropylene phantoms at 80, 100, 120 and 140 kVp tube voltages was 1.03, 0.4, 0.22, 0.15 and 6.46, 2.53, 1.3, 0.8, respectively. Figure 6 shows the integrated SPR (the sum of SPRs in each detector channel located in one detector row) for all detector rows when the water-filled phantom is exposed to various tube voltages. Only the fitted curves are shown for clarity.

4. Discussion

The assessment of x-ray scatter magnitude and spatial distribution is performed in most cases using deterministic methods and simplifying approximations developed mainly to improve the speed of operation. Monte Carlo calculations offer the possibility of estimating physical parameters including x-ray scatter that are difficult or even impossible to calculate

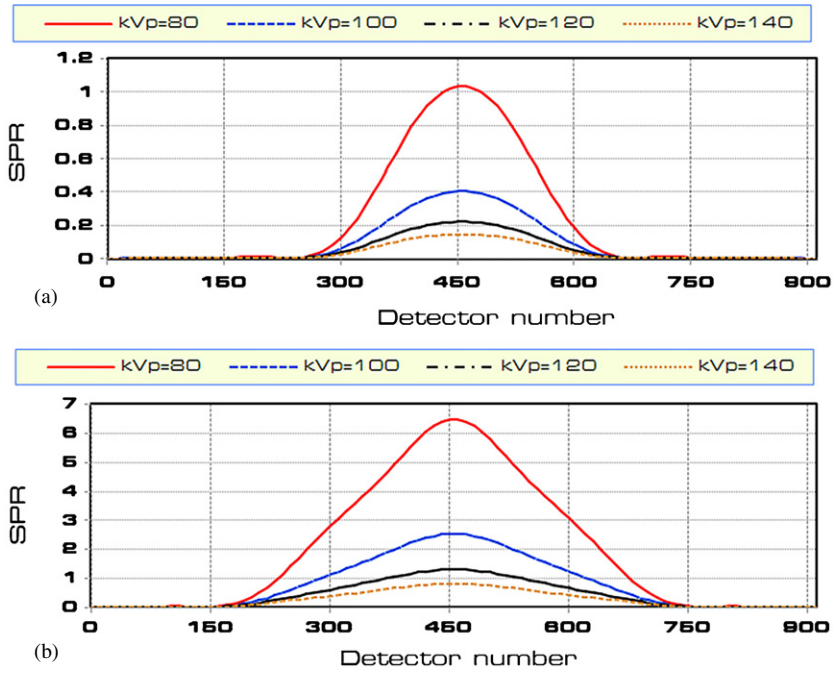

Figure 5. SPR curves for 32nd row of detectors calculated using the blocker array method for various tube voltages for the (a) water phantom and (b) polypropylene phantom.

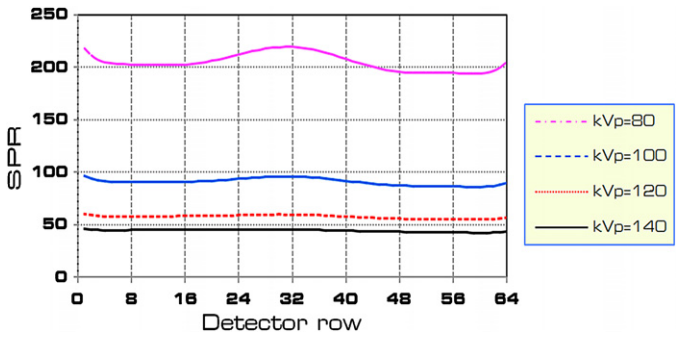

Figure 6. SPR curves obtained from integration of all 912 SPR values of detector elements in each row after curve fitting for tube voltages of 80–140 kVp.

using experimental measurements and analytical modelling. Recent developments in instrumentation and experimental techniques make it possible to characterize accurately the scatter component in x-ray CT and its impact on image quality and quantitative accuracy in dual-modality PET/CT imaging (Ay and Zaidi 2006).

Experimental measurements although necessary for benchmarking are usually prone to error which makes their accuracy questionable. First, contribution from off-focal radiation might contaminate the measured scatter data thus affecting the obtained results. In addition, 'secondary collimator' and other system components above it produce additional scatter radiation. Blocker-based methods inherently induce supplementary sources of scattered radiation as the blocker is itself another added source of scatter and affects the pattern of

scatter distribution. Off-focal radiation can be estimated through additional experiments; however, there is a lack of reliable experimental techniques for the remaining sources of additional scattered radiation. The collimator shadow technique was considered as 'gold standard' in this study since it is the most immune to primary photons which pollute the measured scatter. The lack of thorough substantiation of this technique is recognized and justified by the difficulty of experimental validation of the method. In-depth Monte Carlo simulation studies might be useful in this context and are being investigated for this purpose.

In comparison with the collimator shadow technique used as reference, the mean relative error for the blocker array method is $1.4 \pm 1.1\%$ (with a maximum value of 5%) whereas it is $3.9 \pm 3.6\%$ (with a maximum value of 20%) for the single blocker method. The larger error for the latter approach is inherent to the principle of the single blocker method which estimates the scatter profile by rotating the source around the phantom. Under these conditions, the distance between the blocker and the source is altered which results in overestimation of the scatter profile.

Since the blocker array method is relatively straightforward and easy to use for extracting the scatter and primary profiles, the SPR curve was calculated for all tube voltages. Despite the limited accuracy of this approach outside the phantom shadow area, the method is reliable for calculation of the SPR since a very high number of primary photons are recorded which undermine the impact of such inaccuracies outside the phantom shadow area. The SPR estimates for high tube voltages are lower than those for low tube voltages (figure 5). This can be explained as follows: as tube voltage increases, the rate of increase of primary photons (denominator in the SPR equation) is much higher than the rate of decrease of scattered photons (numerator in the SPR equation). Therefore, the scatter-to-primary ratio becomes smaller when increasing the tube voltage.

The integration of SPR curves for each individual detector row results in relatively high intensity in the central rows (figure 6) since these central rows record the scatter contribution emanating from both sides of detector rows. By observing the SPR in different rows of the detector, it appears that the SPR goes down from row 1 up to row 64, resulting in an asymmetric SPR curve. This can be explained by the 'anode heel' effect which causes the number of primary photons in rows close to row 64 to be higher than that in far away rows. Hence, the SPR decreases for rows close to row 64.

The effect of the bowtie filter on the SPR remains an open research question which is being investigated and will be reported in future work. In addition, characterization of the scatter component in non-homogeneous human-like anthropomorphic phantoms still requires further research and development efforts.

An accurate and robust assessment of the SPR pattern is the key factor for implementation of model-based scatter correction algorithms. Therefore, the experimental techniques of scatter estimation studied in this work may play an important role in the development of scatter correction algorithms. Considering their pros and cons, the collimator shadow method seems to be suitable for single-slice scanners while the blocker array method is promising and might be an appropriate choice for calculation of the SPR in multi-slice and cone-beam scanners owing to its simplicity and ease of use.

5. Conclusion

Three different experimental methods for calculation of the scatter profile in volumetric x-ray CT were examined and compared in this study. The collimator shadow method is by far the most accurate empirical technique of choice. However, this approach is not practical for the cone-beam geometry with wide collimator aperture and when the object is inhomogeneous.

The blocker-based methods are not suitable when the object under study has low linear x-ray attenuation; however, these techniques provide a straightforward approach for scatter estimation provided the additional exposure to the patient can be neglected. Moreover, the proposed blocker array method is a robust approach for experimental calculation of the SPR even for cone-beam CT scanners.

The aforementioned scatter estimation techniques could serve as a basis for development of novel scatter correction algorithms to improve CT image quality and quantitative accuracy and also to reduce the impact of scatter-related artefacts. In addition, since CT images play a key role for attenuation correction of PET data on hybrid PET/CT scanners, accurate x-ray CT scatter correction will play a significant role in future designs of this technology with a larger axial field of view.

Acknowledgments

This work was supported by Tehran University of Medical Sciences under grant no 132-5288 and the Swiss National Foundation under grant no 31003A-125246.

References

Akbarzadeh A, Ay M R, Ghadiri H, Sarkar S and Zaidi H 2008 A novel approach for experimental measurement of scatter profile and scatter to primary ratio in 64-slice CT scanner *4th Kuala Lumpur Int. Conf. on Biomedical Engineering 2008 (IFMBE Proc.* vol 21*)* (Berlin: Springer) pp 473–7

Ay M R and Zaidi H 2005 Development and validation of MCNP4 C-based Monte Carlo simulator for fan- and cone-beam x-ray CT *Phys. Med. Biol.* **50** 4863–85

Ay M R and Zaidi H 2006 Assessment of errors caused by x-ray scatter and use of contrast medium when using CT-based attenuation correction in PET *Eur. J. Nucl. Med. Mol. Imaging* **33** 1301–13

Bertram M, Wiegert J and Rose G 2005 Potential of software-based scatter corrections in cone-beam volume CT *Proc. SPIE* **5745** 259–70

Colijn A P and Beekman F J 2004 Accelerated simulation of cone beam x-ray scatter projections *IEEE Trans. Med. Imaging* **23** 584–90

Endo M, Mori S, Tsunoo T and Miyazaki H 2006 Magnitude and effects of x-ray scatter in a 256-slice CT scanner *Med. Phys.* **33** 3359–68

Endo M, Tsunoo T, Nakamori N and Yoshida K 2001 Effect of scattered radiation on image noise in cone beam CT *Med. Phys.* **28** 469–74

Glover G H 1982 Compton scatter effects in CT reconstructions *Med. Phys.* **9** 860–7

Johns P C and Yaffe M 1982 Scattered radiation in fan beam imaging systems *Med. Phys.* **9** 231–9

Kalender W A 1988 New developments in bone density measurement by quantitative computer tomography *Der Radiologe* **28** 173–8

Kanamori H, Nakamori N, Inoue K and Takenaka E 1985 Effects of scattered x-rays on CT images *Phys. Med. Biol.* **30** 239–49

Li H, Mohan R and Zhu X R 2008 Scatter kernel estimation with an edge-spread function method for cone-beam computed tomography imaging *Phys. Med. Biol.* **53** 6729–48

Maltz J S, Gangadharan B, Bose S, Hristov D H, Faddegon B A, Paidi A and Bani-Hashemi A R 2008a Algorithm for x-ray scatter, beam-hardening, and beam profile correction in diagnostic (kilovoltage) and treatment (megavoltage) cone beam CT *IEEE Trans. Med. Imaging* **27** 1791–810

Maltz J S *et al* 2008b Focused beam-stop array for the measurement of scatter in megavoltage portal and cone beam CT imaging *Med. Phys.* **35** 2452–62

Malusek A, Sandborg M and Carlsson G A 2003 Simulation of scatter in cone beam CT—effects on projection image quality *Proc. SPIE* **5030** 740–51

Malusek A, Sandborg M and Carlsson G A 2008 CTmod—a toolkit for Monte Carlo simulation of projections including scatter in computed tomography *Comput. Methods Programs Biomed.* **90** 167–78

Ning R, Tang X and Conover D 2004 X-ray scatter correction algorithm for cone beam CT imaging *Med. Phys.* **31** 1195–202

Ohnesorge B, Flohr T and Klingenbeck-Regn K 1999 Efficient object scatter correction algorithm for third and fourth generation CT scanners *Eur. Radiol.* **9** 563–9

Rinkel J, Gerfault L, Esteve F and Dinten J M 2007 A new method for x-ray scatter correction: first assessment on a cone-beam CT experimental setup *Phys. Med. Biol.* **52** 4633–52

Siewerdsen J H, Daly M J, Bakhtiar B, Moseley D J, Richard S, Keller H and Jaffray D A 2006 A simple, direct method for x-ray scatter estimation and correction in digital radiography and cone-beam CT *Med. Phys.* **33** 187–97

Siewerdsen J H and Jaffray D A 2000 Optimization of x-ray imaging geometry (with specific application to flat-panel cone-beam computed tomography) *Med. Phys.* **27** 1903–14

Siewerdsen J H and Jaffray D A 2001 Cone-beam computed tomography with a flat-panel imager: magnitude and effects of x-ray scatter *Med. Phys.* **28** 220–31

Sorenson J A and Floch J 1985 Scatter rejection by air gaps: an empirical model *Med. Phys.* **12** 308–16

Tofts P S and Gore J C 1980 Some sources of artefact in computed tomography *Phys. Med. Biol.* **25** 117–27

Yao W and Leszczynski K W 2009 An analytical approach to estimating the first order x-ray scatter in heterogeneous medium *Med. Phys.* **36** 3145–56

Zaidi H and Ay M R 2007 Current status and new horizons in Monte Carlo simulation of x-ray CT scanners *Med. Biol. Eng. Comput.* **45** 809–17

Zhu L, Bennett N R and Fahrig R 2006 Scatter correction method for x-ray CT using primary modulation: theory and preliminary results *IEEE Trans. Med. Imaging* **25** 1573–87

Zhu L, Xie Y, Wang J and Xing L 2009 Scatter correction for cone-beam CT in radiation therapy *Med. Phys.* **36** 2258–68